StoppedFlow 19F NMR Spectroscopic Analysis of a Protodeboronation Proceeding at the SubSecond TimeScale

EurJOC
European Journal of Organic Chemistry

Full Papers
doi.org/10.1002/ejoc.202100290

Chemistry Europe
European Chemical Societies Publishing

Stopped-Flow ^{19}F NMR Spectroscopic Analysis of a Protodeboronation Proceeding at the Sub-Second Time-Scale

Ran Wei,[a] Andrew M. R. Hall,[a] Richard Behrens,[b] Mark S. Pritchard,[c] Edward J. King,[c] and Guy C. Lloyd-Jones*[a]

In-situ NMR spectroscopic analysis of homogeneous reactions is an essential tool for mechanistic analysis in organic and organometallic chemistry. However, rapid non-equilibrium reactions, that are initiated by mixing, require specialized approaches. We report herein on a study of the factors that ensure quantitative results in a recently-developed technique for stopped-flow NMR spectroscopy. The influence of some of the key parameters on quantitation is studied by ^{19}F NMR spectroscopic analysis of the kinetics and activation parameters for the base-catalyzed protodeboronation of highly-reactive polyfluorinated arylboronic acids, with half-lives as low as 0.1 seconds. The effects of spin relaxation, pre-magnetization, heat-transfer versus reaction enthalpy, and mixing-efficiency are analyzed in detail. We also compare and contrast choice of pulse angle, interscan delay, and use of pseudo real-time by interleaving, as means to achieve an optimal balance between temporal resolution and sensitivity.

Introduction

The elucidation of chemical reaction mechanisms is essential for the informed optimization of known processes, and a powerful impetus in the design of new ones.[1] Tracing the components of a reaction, and the chronology of their evolution,[2] offers invaluable insights, including identification of intermediates, side-products, and catalysts, and quantification of selectivity. Techniques for determining reaction kinetics should ideally a) provide structural information for identification of chemical species evolving throughout the reaction; b) allow straightforward quantitation of concentrations; and c) be applicable under the conditions under which the reaction of interest is usually employed (concentration, solvent, temperature, etc.). In general, *in-situ* NMR spectroscopy fulfils all of the requirements outlined above and is applicable to a broad range of nuclei common in organic and organometallic reactions. Indeed, with spectrometers ubiquitous in chemistry departments, NMR spectroscopy offers such a wealth of information that it remains one of the most widely utilized techniques for kinetic analysis of organic reactions.

Reactions that proceed 'slowly', by which we mean half-lives, $t_{1/2}$, on the order of 30 seconds or more, can be studied by routine NMR techniques.[3] However, those that are 'rapid' require a more specialized approach. Rapid reactions can be divided into two classes (Scheme 1): systems at equilibrium and systems that evolve irreversibly after initiation. The analysis of rapid equilibria by NMR spectroscopy using line-shape analysis,[4–6] magnetization or saturation transfer experiments,[7,8] and spin-echo[9–11] or CPMG methods,[12,13] is well-established. For example, SHARPER[14] allows activation parameters to be derived from temperature-dependent line-broadening and distortion effects, and the CPMG spin-echo pulse sequence reveals protein motions at microsecond to millisecond timescale.[15,16] However, monitoring rapid *irreversible* reactions by NMR spectroscopy poses a considerably different challenge,

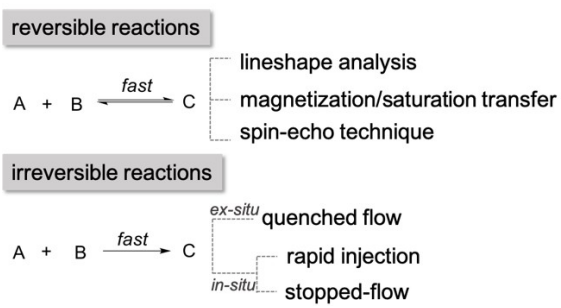

Scheme 1. Generic NMR analysis techniques for the kinetics of reversible, and irreversible, rapid reactions A + B = C. Herein 'fast' refers to reactions with (pseudo) first-order half-lives, $t_{1/2}$, on the order of seconds or lower.

[a] *R. Wei, Dr. A. M. R. Hall, Prof. Dr. G. C. Lloyd-Jones*
School of Chemistry
The University of Edinburgh
Joseph Black Building, David Brewster Road, Edinburgh, EH9 3FJ, UK
E-mail: guy.lloyd-jones@ed.ac.uk
http://www.lloyd-jones.chem.ed.ac.uk
[b] *Dr. R. Behrens*
Laboratory of Engineering Thermodynamics (LTD)
Technische Universität Kaiserslautern
Erwin-Schrödinger-Straße 44, Kaiserslautern, 67663, Germany
[c] *M. S. Pritchard, E. J. King*
TgK Scientific Ltd.
Bradford on Avon, Wiltshire, BA15 1DH, UK
http://www.hi-techsci.com

Supporting information for this article is available on the WWW under https://doi.org/10.1002/ejoc.202100290

especially when such processes are initiated by mixing, rather than by a readily controlled external stimulus such as light.[17]

Over the last decade we have investigated a wide range of anion-mediated processes involving organoboron[18–21] and organosilicon[22–26] reagents, including hydrolytic activation and degradation of boronic acids,[18,21] and their derivatives.[19,20] In the majority of examples we were able to employ standard ^{1}H, ^{11}B, ^{19}F, and ^{29}Si NMR spectroscopic techniques to analyze the reaction kinetics. However, some reactions, for example the protodeboronation of polyfluorophenylboronic acids, **1**, Scheme 2,[21] required fast *in-situ* spectroscopic techniques, such as SF-FT-IR, or very rapid *ex-situ* quench methods.[27–29]

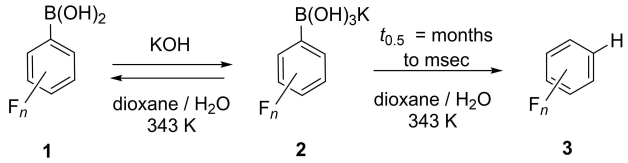

Scheme 2. Base-catalyzed protodeboronation of polyfluorophenyl boronic acids, with half-lives ranging from 7 months (3-fluorophenylboronate) to 2.6 milliseconds (2,3,4,5,6-pentafluorophenylboronate).[21]

Results and Discussion

Whilst the IR/quench techniques allowed us to determine a wide range of protodeboronation kinetics, $n = 0$ to 5, Scheme 2, they did not provide the key insights that NMR spectroscopy can. These aspects led us to explore application of the two general techniques to monitor relatively fast irreversible reactions by NMR: rapid-injection,[30–35] and stopped-flow,[36–43] Figure 1. The primary difference between the two techniques lies in the way they mix the analytes. For rapid-injection methods, a solution containing the final reagent(s) needed to initiate the reaction is injected at high speed into an NMR tube containing the remainder of the reagents, using the tube itself as the

Ran Wei conducted her undergraduate studies at the University of Science and Technology Beijing, in 2010. She obtained her Master's degree in Chemistry from the University of Manchester, during which period she undertook her MSc project focusing on pure shift NMR and developed her interest in this area. In 2019 she joined the Lloyd-Jones group as a PhD student, her work primarily focuses on new NMR methods and their application in physical-organic mechanistic investigations.

Andrew Hall graduated from Imperial College, London with an MSci in Chemistry in 2014. He then moved to the University of Bath to carry out an integrated PhD at the Centre for Sustainable Chemical Technologies, under the supervision of Dr Antoine Buchard and Dr Ulrich Hintermair. After completing his PhD in 2018 he carried out postdoctoral studies in the group of Dr Giuseppe Pileio at the University of Southampton, before moving to the University of Edinburgh in January 2020. His research in the Lloyd-Jones group focuses on the development of new stopped-flow instrumentation for monitoring fast reactions by NMR spectroscopy.

Richard Behrens obtained his Bachelor's degree from FH Kaiserslautern and his Master's degree in mechanical engineering with a specialization in fluid process engineering from TU München in 2014. He then worked at the Laboratory of Engineering Thermodynamics at TU Kaiserslautern under the supervision of Prof. Erik von Harbou and Prof. Hans Hasse. In 2018, he visited the Lloyd-Jones group as guest researcher to compare and contrast stopped-flow NMR designs at Kaiserslautern and Edinburgh. Richard received his PhD in 2019 and is currently working at BASF SE in Ludwigshafen in the process research department for gas scrubbing.

Mark Pritchard is an electronics engineer with a wide range of experiences in the mechanical and electronic design of scientific instruments and specialist products for chemistry and the bio-physical sciences. He has specialized in design techniques and project management and has made major contributions to the development of IR and NMR projects in the Lloyd-Jones group Edinburgh.

Edward ('Ted') King is a chartered engineer with a wide range of experiences and knowledge; especially in the design of scientific instruments and specialist products for chemistry and the bio-physical sciences. With a strong background in UV/Vis, IR, and fluorescence spectroscopy and related physical methods applied to fast reactions in solution, his interests have more recently expanded to NMR, through a rich and productive collaboration with the Lloyd-Jones group at the University of Edinburgh.

Guy Lloyd-Jones studied Chemical Technology at Huddersfield Polytechnic, obtained his doctorate at Oxford with John Brown FRS, did postdoctoral research with Andreas Pfaltz at Basel, and began his independent career in 1996 at Bristol. In 2013 he moved to the Forbes Chair of Organic Chemistry at the University of Edinburgh. Over the last 25 years his research has focused on the mechanism and kinetics of synthetic processes and reactions, and more recently on the development of new methods for UV, IR and NMR analysis, in a series of highly productive collaborations with Ted King and Mark Pritchard.

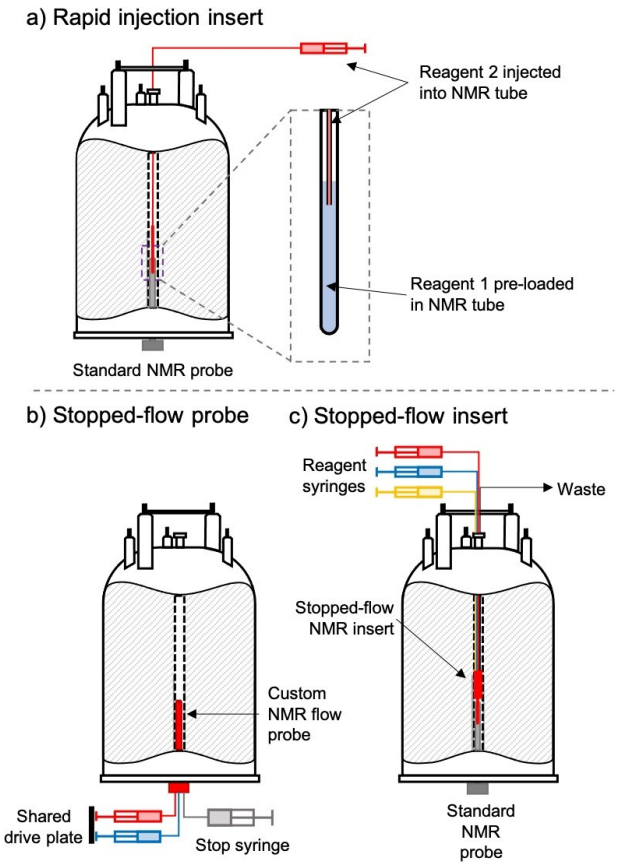

Figure 1. Schematic representations of a) rapid injection apparatus designed to insert into a standard NMR probe, b) a customized stopped-flow probe, and c) a stopped-flow apparatus designed to insert into a standard NMR probe.

mixing chamber, Figure 1a. In the stopped-flow technique the reactants are passed through a mixing device and the nascent reaction mixture delivered to an NMR flow cell, Figure 1b, Figure 1c.

Stopped-Flow NMR. Since the first reports of stopped-flow NMR spectroscopy techniques in the 1970s,[36–38] there has been a focus on minimizing the phenomenological dead-time: the time duration between the initiation of the reaction and the start of data acquisition. There are three main contributors to the dead-time in a stopped-flow NMR experiment: i) mixing, ii) transport from the mixer to the NMR flow cell, and iii) cessation of flow and pressure oscillations. An early publication from Ernst et al.[38] highlighted the potential of stopped-flow NMR in detecting fast irreversible reactions, despite the limitations of instrumentation at the time, and line-shape distortions caused by oscillations induced by the rapid ('hard') stopping motion. More recent developments have included rapid mixing cells using pneumatic drives and solenoid valves,[40] customized probes for greater reagent polarization and temperature control,[42–44] and high pressure stopped-flow devices.[39] Landis and Christianson have also reported simulations of the changes in intensity, line-width, and phase, in NMR spectra arising from very rapid reactions.[45]

In 2018 we reported on a detailed study of the mechanism of anion-initiated CF_3 transfer from $TMSCF_3$[23] in which we employed a stopped-flow insert (Figure 1c) that we custom-built for the investigation. In our subsequent analyses of CF_2 generation,[24] and arene C–H silylation by $TMSCF_3$,[46] we have optimized our design and use of the stopped-flow system. Herein we report in detail on the physical and NMR parameters that help enable quantitative and accurate kinetics when implementing the technique, using the rapid protodeboronation (Scheme 2) of 2,3,4,6-tetrafluorophenyl boronic acid **1a**, and 2,3,4,5,6-pentafluorophenyl boronic acid **1b**, as challenging examples for analysis.[21,47]

General Design Features. There are a number of distinct features between the approach discussed herein (Figure 2b) and the conventional design for stopped-flow NMR spectroscopy (Figure 2a). The major difference is the use of three independent drive syringes, thereby allowing systematic variation in reagent concentrations, using a single set of stock solutions (A, B, C). The use of computer-controlled drives allows the flow to be stopped by the resistance present in the open-ended circuit (see 'waste' in Figure 2b) after arresting the movement of the drives. The trigger signal is sent to the NMR console from the syringe drive unit, rather than from a microswitch on a stop syringe. This configuration reduces the acute pressure and flow oscillations induced by the 'hard stop' of a classic stop-syringe (Figure 2a). In both designs (Figure 2a, Figure 2b) reactant nuclei are polarized in pre-magnetization reservoirs (see later) placed immediately before the mixer. The latter employs a sufficiently high flow-rate to generate turbulence and enable the efficient mixing required to initiate the reaction with a clearly defined start point. The flow is also used to purge the previous contents from the sample cell and replace it with the nascent reaction mixture primed for NMR spectroscopic measurement. Herein we have employed flow rates ranging from 0.2 mL/s to 2 mL/s, resulting in dead-times ranging from 0.75 to 0.075 seconds, respectively, to prime the 3 mm outer-diameter 180 μL capacity glass flow-cell. The capacity of the flow-cell in the detection region of the NMR receiver coil is approximately 93 μL and this results in about 3-fold lower S/N compared to a normal 5 mm NMR tube. However, in contrast to custom-built stopped-flow NMR probes (Figure 1b), the system described herein is inserted directly into a standard NMR probe head (Figure 1c) allowing use of highly-sensitive He or N_2 cryoprobes.

Establishing the Boltzmann Distribution. In conventional NMR spectroscopy, a Boltzmann distribution of spin populations is developed in the analyte solution in the probe-head at the center of the magnetic field (B_0) of the spectrometer. Radio-frequency (RF) pulses applied at a direction perpendicular to B_0 disturbs this distribution, and it is the relaxation of the excited spins back to equilibrium that gives rise to the NMR signal. Whilst it takes a significant time for the spins to develop their initial Boltzmann distribution (99% equilibration requires $5 \times T_1$), in routine NMR spectroscopy this 'pre-magnetization' occurs during the pre-acquisition processes of locking, shimming and tuning, after the sample tube has been inserted into the spectrometer.

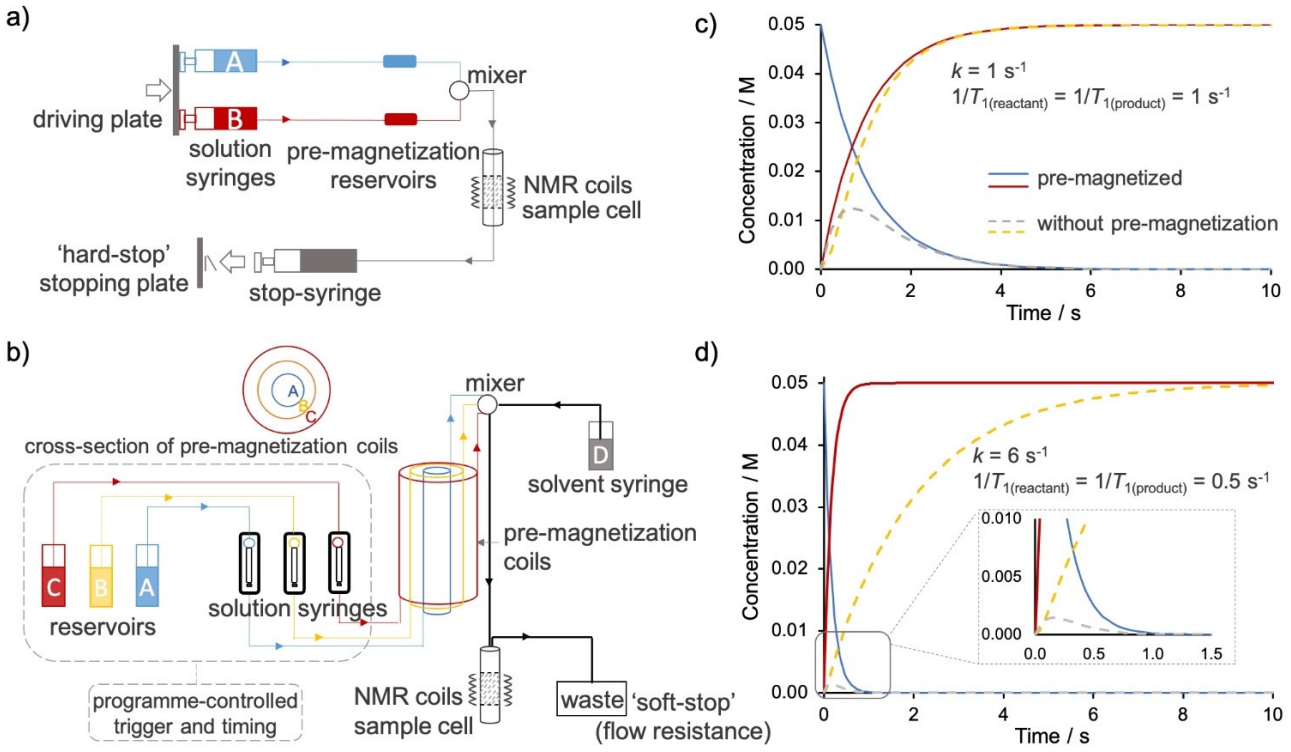

Figure 2. Schematic representations of a) classical dual-input 'hard-stop' stopped-flow apparatus, and b) variable-ratio triple input 'soft-stop' stopped-flow apparatus; see text for full discussion. c) A simulated first-order reaction profile (reactant→product) showing the difference between the real concentrations (solid lines) versus those determined from the intensity of NMR signals arising from non-pre-magnetized reactants (dashed lines), when the reaction rate (k) is the same as the longitudinal relaxation rate ($1/T_1$). d) An analogous simulation where $k \gg 1/T_1$. Inset: magnification of the first 1.5 seconds; see text for full discussion.

The solid lines in Figure 2c show the temporal concentration profiles for a first-order process ('reactant'→'product') where $kT_1 = 1$. The dashed lines show the apparent concentrations that would be determined based on the NMR signal intensities when the reaction is initiated *without* prior establishment of the Boltzmann distribution of spins (for details see the SI), indicative of a major underestimation of the reactant concentration. When the reaction rate substantially exceeds the relaxation rates of the studied spins (e.g. Figure 2d, $kT_1 = 12$) the NMR signal for the reactant can barely be detected, as it is consumed more rapidly than it is magnetized. Moreover, the NMR signal for the product predominantly reflects the magnetization process, not the change in concentrations due to the chemical reaction of interest.

Thus, for stopped-flow NMR analysis of reactions that proceed faster than the Boltzmann distributions of the various nuclei involved can be achieved, attaining signal intensities that directly reflect concentrations requires that the reaction components are exposed to the magnetic field (B_0) for $> 5 \times T_1$ *before* the reaction is initiated by mixing. Unlike the NMR spectrometers employed in the early stages of development of stopped-flow techniques,[36–38] modern superconducting magnets have very little stray field. Thus, the reactants must be pre-magnetized in reservoirs located as close as possible to the field-center and the NMR probe head.

Pre-magnetization. In the system shown in Figure 2b polarization of the reactants (A, B, C) is achieved by a set of three pre-magnetization reservoirs located just above the probe head, see Figure 3. This has the potential to afford high (but in contrast to bespoke probe heads, Figure 2a, not complete) polarization of the nuclei in the reactants before they are mixed and delivered to the flow-cell. The extent of the polarization (Figure 3a) differs mainly based on the delivered volumes and the concentric arrangement of the coil-shaped reservoirs (Figure 3b). Since a total delivered volume (A + B + C) of ≥ 600 μL is required to fully purge the previous sample and refill the flow-cell with nascent reaction mixture, the pre-magnetization profile allows definition of the limits in individual delivery volumes (A, B, C) to afford > 90 % pre-magnetization.

Mixing efficiency. Rapid mixing is essential in all stopped-flow experiments to ensure a well-defined reaction start time. The system employed herein passes the reagent streams (A, B, C) through a passive micromixer and down to the reaction flow-cell through a narrow bore glass capillary, ideally as a homogeneous reaction mixture. To assess this aspect, the mixing time was estimated by spectrophotometry using the Villermaux-Dushmann protocol.[48,49] This method uses competing iodate/iodine and acid/base reactions, where the concentration set is chosen such that in a well-mixed sample the acid is entirely neutralized by a fast reaction with the borate buffer before any iodine is formed. In a poorly mixed sample, pockets

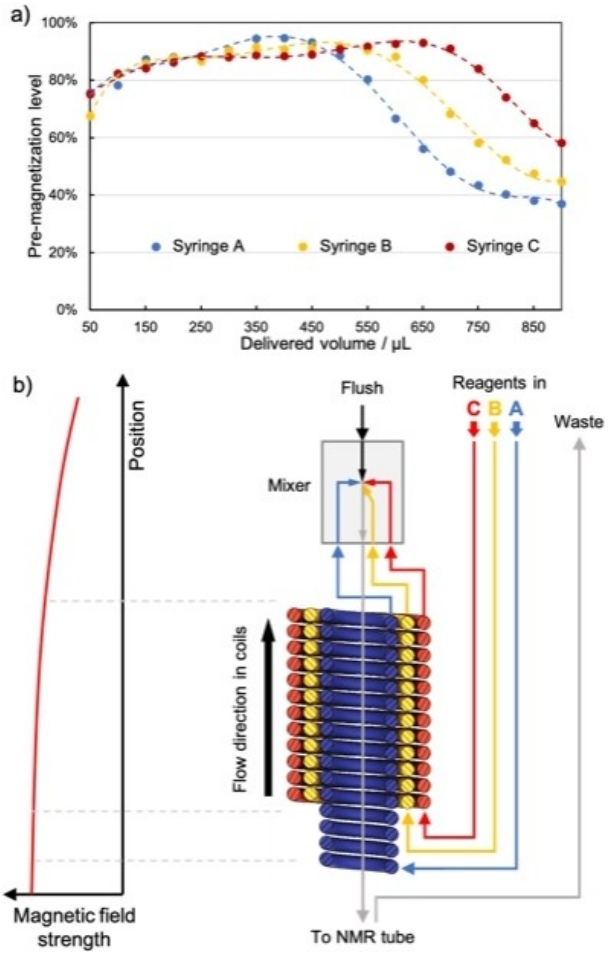

Figure 3. a) Pre-magnetization profiles of input solutions A, B, C. Volumes ranging from 50–900 µL in increments of 50 µL were studied, the dashed lines through the datapoints are for visual guidance only. b) vertical cross-section of the pre-magnetization reservoirs. The reagents from solution syringes flow through the pre-magnetization coils in an upward manner until they reach the mixer. The homogeneously mixed volume is then delivered back down to the flow-cell in the probe head at the magnetic field center. The relative vertical position of the coils to NMR probe and the corresponding magnetic field strength experienced are illustrated in the left-hand section of the figure.

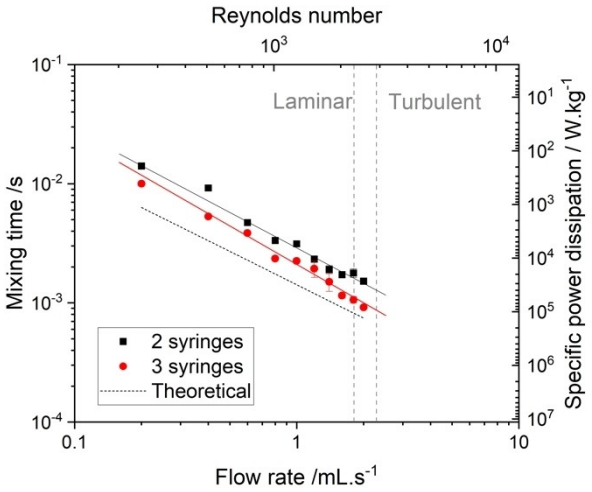

Figure 4. Mixing time characterization as a function of flow rate through the mixer (Figure 3b), estimated using the Villermaux-Dushmann method.[48,49] Transitions between laminar and turbulent flow regimes in the mixer were estimated using the Reynolds number calculated for water using the nominal dimensions of the mixer. The specific power dissipation of the mixer was estimated from the mixing time as described by Falk.[50]

of high acid concentration are only partially neutralized by the buffer, allowing the slower iodate/iodine reaction to occur. The concentration of iodine was measured by UV-Vis spectrophotometry and the mixing time was estimated using a model derived from known reaction rates and ionic strengths.[48,50]

$$H_4BO_4^- + H^+ \rightarrow H_3BO_3 + H_2O$$
$$IO_3^- + 5I^- + 6H^+ \rightarrow 3I_2 + 3H_2O$$

The mixing time for the system employed herein (Figure 2b and Figure 3) was determined to be between 0.9 and 14.1 milliseconds (Figure 4); a range comparable to other similarly sized micromixers.[50] As expected, the mixing time is inversely proportional to flow rate, with higher flow rates resulting in greater power dissipation and more-efficient mixing. The mixing time is between 4 and 9 times shorter than the residence time, meaning that the sample is fully mixed by the time it exits the mixer. Using three inputs (A, B, C) resulted in slightly shorter mixing times than using only two (A, B), likely due to parallel lamination of the reagent streams.[51]

Reaction Enthalpy. One of the advantages of custom-built stopped-flow NMR probes (Figure 1b) is that a single, highly-effective, fluid-based thermostatting system can be incorporated in the probe head where the reaction is conducted.[42,43] In contrast, a system based on insertion of a stopped-flow cell into a standard NMR probe (Figure 1c) requires two thermostatic systems. An auxiliary system provides thermostatting to the pre-magnetization, mixing, and sample transport stages,[52] with control transitioning to the spectrometer during measurement. For the work herein we used an aqueous ethylene glycol heat transfer medium, and a Pt100 temperature probe located close to the mixer to pre-calibrate the auxiliary system to be within ±0.5 K of the spectrometer thermostat. After delivery of the nascent reaction to the NMR flow-cell and cessation of the flow, the reaction temperature must remain sufficiently stable to provide reliable kinetic data. Standard NMR spectrometers use gas flow (dry air or N_2) to stabilize the temperature of analyte solutions in 5 mm NMR tubes, a system that is not designed to regulate fast process with large enthalpies of reaction.

To evaluate the limits of the spectrometer thermostat, we used the technique of von Harbou et al. to estimate the error in the apparent rate constant for a reaction, as a function of its half-life, enthalpy change, and concentration.[43] We first determined the heat transfer coefficient from the flow-cell to the surrounding gas-flow in the spectrometer. Methanol was heated to 50 °C using the auxiliary system, and then delivered via a standard stopped-flow 'shot' to the 3 mm glass NMR tube flow-cell that had been pre-heated to 30 °C in the spectrometer gas flow (Figure 5a). The cooling rate (Figure 5b) was estimated

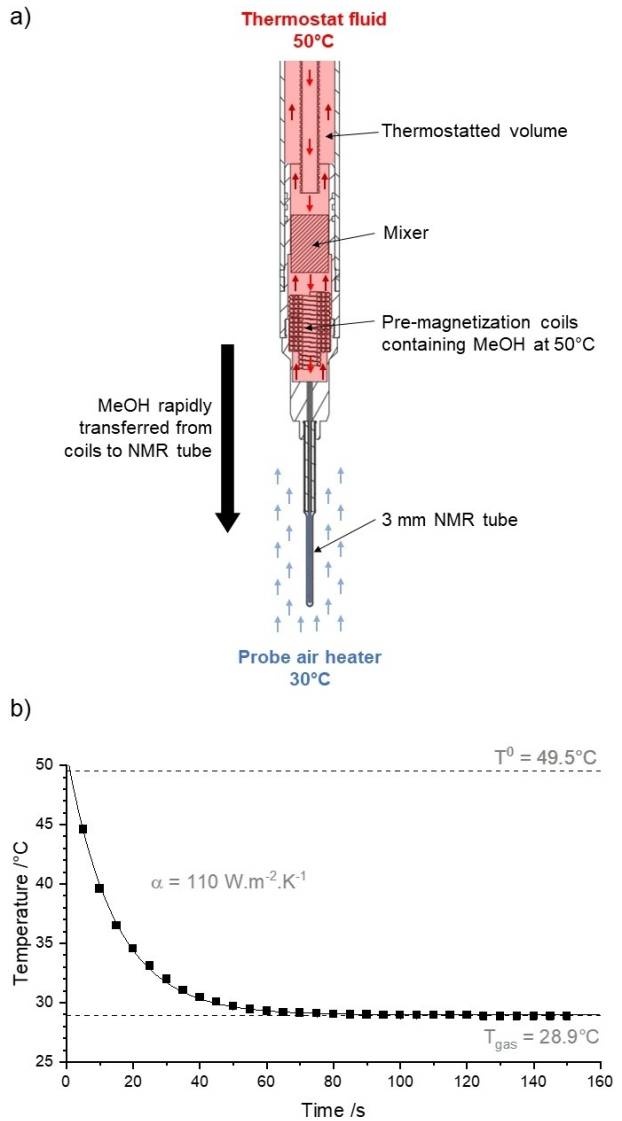

Figure 5. a) Experimental determination of the heat transfer coefficient using the methanol NMR thermometer technique.[53] The co-axial thermostat circuit is analogous to that of a known continuous-flow NMR system.[54] b) Temperature evolution of pre-heated methanol upon injection into the flow-cell including fitted parameters; the air flow-rate was 535 L/h.

using the ^{1}H NMR chemical shift difference between CH_3/OH protons.[53] With the assumption that heat transfer from the methanol occurs by radial conduction, the heat transfer coefficient, (α, 110 $W m^{-2} K^{-1}$) was then determined from the flow-cell dimensions, and standard properties of the methanol (see SI).

A chemical reaction that proceeds with a substantial enthalpy change will establish a radial temperature gradient in the reaction medium, thus leading to a radial gradient of the rate of reaction, and in turn to a radial concentration gradient. The impact of this effect on the measured versus real rates of reaction for a generic first-order process was evaluated using the Arrhenius equation. All properties (heat conductivity, enthalpy of reaction, heat capacity, etc.) were considered to be constant. The energy and component balances result in three coupled partial differential equations of the concentration and the temperature of the reactants, and of the temperature of the glass of the NMR flow cell. The partial differential equations were solved numerically (see SI) and used to construct a non-isothermal model, at four different initial concentrations of substrate, Figure 6a–d.

The results show that unless the reaction is very exothermic, the standard spectrometer thermostat system (Figure 5a) provides sufficient control for reactions with half-lives as low as 100 msec, when the initial concentration is 0.05 M (Figure 6b) or lower. Higher concentrations can be used for weak to moderately exothermic reactions, affording enhanced sensitivity without compromising the accuracy of the kinetics.

Longitudinal Relaxation. The relaxation time constant T_1 is an essential but sometimes overlooked parameter for consideration in NMR kinetic studies, especially for rapid reactions when data acquisition needs to be repeated in a relatively short time window. For quantitative NMR, T_1 constants govern the repetition rate between successive acquisitions in the basic experiment for reaction monitoring (Figure 7a). In general, an interscan delay, t_R, of $5\times T_1$ is necessary to recover $>99\%$ of the magnetization between the application of 90° pulses. Using an interscan delay that is too short will result in incomplete relaxation of the nuclei between scans and saturation of some or all signals, which compromises quantification.

One approach is to use smaller pulse angles, trading reduced sensitivity for enhanced data density. For example, 30° pulses effectively shorten the required interscan delay between two transients to $2.9\times T_1$ for $>99\%$ relaxation recovery, at the penalty of a 50% sensitivity loss compared to using 90° pulses. Use of 10° pulses further enhances the temporal resolution by shortening the interscan delay to just 0.77 $*T_1$, but at the cost of a 6-fold reduction in sensitivity. Therefore, a knowledge of the T_1 constant(s), including that of the internal standard(s), aids selection of acquisition parameters to achieve optimal balance between temporal resolution and sensitivity. Moreover, incomplete pre-magnetization will result in spins continuing to be polarized inside the reaction-cell, in a T_1-dependent manner (Figure 7c). Thus, if the reactants or internal standards have substantially different T_1 constants, unequal magnetization rates will compromise the accuracy of quantification of the data acquired within the reaction period, as discussed below.

Pulse angle, θ, and Sensitivity. Accurate quantitation in NMR requires a high signal-to-noise ratio (S/N), and thus acquisition time, receiver gain, and signal-averaging (number of FIDs) are important parameters. However, in rapid irreversible reactions the analytes evolve too fast to allow signal averaging, constraining the number of FIDs to one per time point. In addition, the interscan delay, t_R, between consecutive pulses determines the data density achievable in a fixed window of time. In our earlier studies,[23,24,46] we routinely used a small radiofrequency pulse angle, typically $\theta = 10°$, to minimize t_R and achieve higher data density, equation (1).[55] Herein, we revised our approach and used θ values optimized for spectral sensitivity (S/N) versus data density, especially in the context of interleaving (see later).

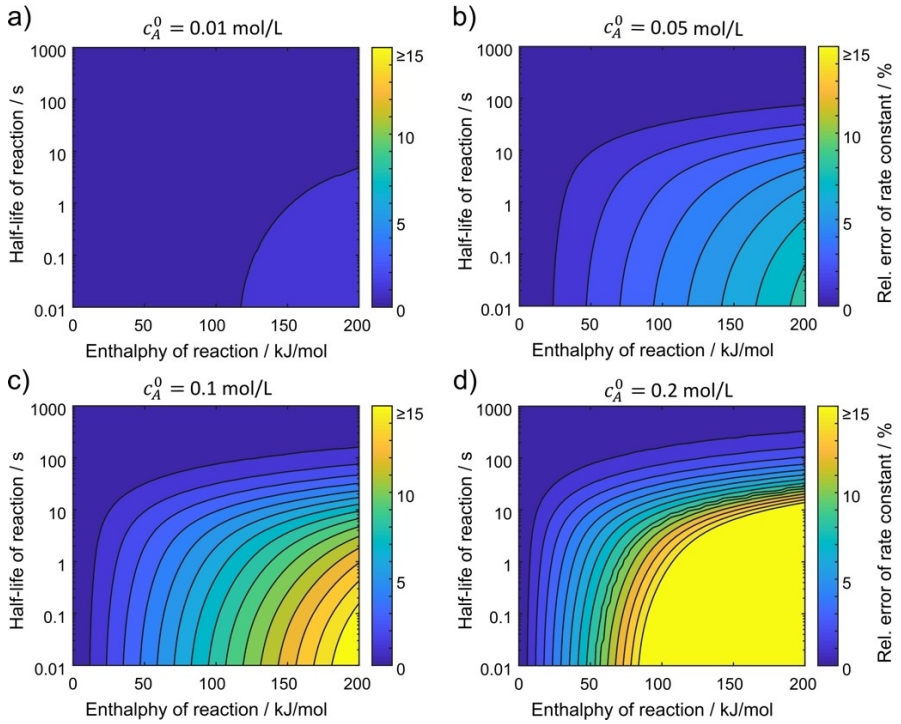

Figure 6. Non-isothermal modelling of a first order reaction (A→P) proceeding in the stopped-flow NMR cell, at four initial concentrations of A. The graphs show the deviation (% - contour scale) of the measured net reaction rate from the real reaction rate that would occur if the sample were thermally homogeneous and at the temperature of gas passed over the external surface of the tube by the spectrometer thermostat system. The x-axis and y-axis show how the deviation varies as a function of reaction half-life and enthalpy. The calculations are based on the empirical heat transfer coefficient Figure 5. See SI for full details.

$$\theta = arccos\left(e^{-t_R/T_1}\right) \quad (1)$$

The half-life of 2,3,4,6-tetrafluorophenyl boronate (**2 a**) generated *in-situ* from boronic acid **1 a**,[21] is 10.4 seconds at 300 K, Figure 8. The calculated enthalpy-change for the process **2 a**→**3 a** is -0.5×10^2 kJmol^{-1} and thus near-isothermal kinetics (Figure 6b) are expected when the initial concentration is 0.05 M or lower.[56] The kinetics (**2 a**→**3 a**, Figure 8) were analyzed by stopped-flow ^{19}F NMR using a variety of pulse angles, θ, with larger angles affording beneficial increases in S/N. However, because of the different longitudinal relaxation rates ($1/T_1$) in the ^{19}F nuclei monitored in the substrate (**2 a**), the internal standard (TFA), and the product (**3 a**), differential signal saturation develops when the pulse angle is too large for the interscan delay, t_R. In the example in Figure 8c, where $\theta = 90°$, this phenomenon leads to a noticeably-distorted reaction profile (compare with Figure 8b), and a significant error in the measured rate constant (see SI).

Sub-second Protodeboronation Kinetics via Interleaving. As is evident from Equation 1, when larger pulse angles, $0 < \theta < 90°$, are employed to gain S/N, the interscan delay, t_R, must be extended to avoid saturation. This in turn leads to lower data density and thus impacts on the quantitation of the kinetics of reactions that proceed faster than the longitudinal relaxation rate, $1/T_1$. We have addressed this by manually enhancing the data density through spectral 'interleaving'. The principle for this is straightforward; the reaction is performed multiple times, incrementing the delay (Figure 7a) between the trigger and the first excitation pulse for each experiment. Data points obtained from separate experiments can then be combined to produce an interleaved dataset.

The process is illustrated schematically in Figure 9 for a reaction that is complete in about 4 seconds. To simulate the spectra, the T_1 constant of the measured species was set to 2 s, and the interscan delay t_R to 1.5 s, with the optimal pulse angle calculated as 60°. Three separate series (blue, red, yellow) were simulated with incremented trigger delays, and each series used to generate one data subset. These three data subsets were combined to generate the final dataset which contains three-fold higher data density. The trigger delays, interscan delay t_R, and pulse angle can be adjusted based on the estimated reaction rate, known T_1 constants, and the required sensitivity and data density. The general stopped-flow method allows reactions to be conveniently and reproducibly initiated as a series of identical 'shots' from the same set of stock solutions. The interleaving experiment solely requires accurate timing of the trigger signal sent to the NMR spectrometer, so that the delay period can be reliably incremented.

We have previously measured the rate of the base-catalyzed protodeboronation of highly-reactive[47] pentafluorophenyl boronic acid **1 b** using the rapid quenched flow technique.[21] The boronate (**2 b**) undergoes the fastest protodeboronation of any

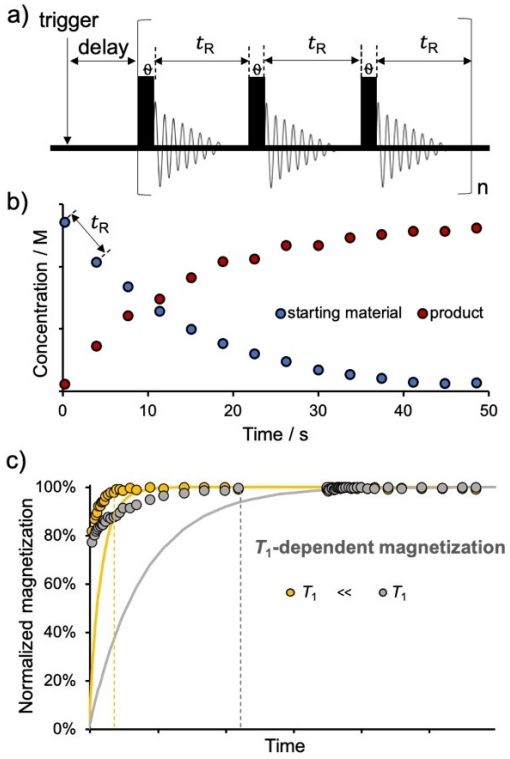

Figure 7. a) pseudo-2D pulse sequence used for reaction monitoring. The pulse angle, θ, and interscan delay, t_R, are adjustable acquisition parameters. b) an example of a first-order reaction profile acquired using the pulse sequence shown in a). c) continued polarization of analytes in the flow tube (circles) after being 'shot' from the stopped-flow solution syringes, and simulated polarization of analytes without pre-magnetization (lines).

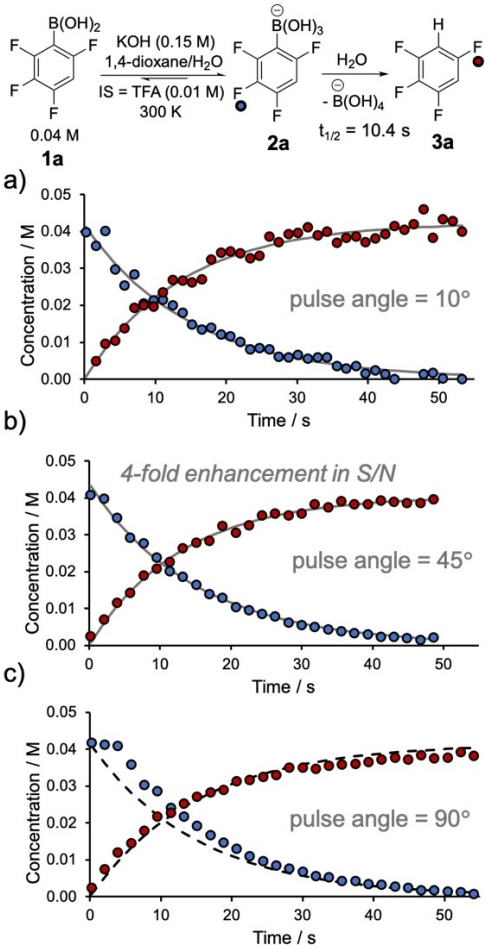

Figure 8. Stopped-flow ^{19}F NMR analysis of the protodeboronation of boronate **2a** (0.04 M) using 10°, 45°, and 90° pulses. In (a) and (b), non-linear regressions of the first-order decay of **2a** were identical ($t_{1/2}$ = 10.4 s). In (c) differential saturation (see text and SI) results in deviation from the true rate (see dashed lines). ^{19}F NMR longitudinal relaxation constants, T_1, blue-labelled F in **2a**, 1.347 ± 0.009 s, red-labelled F in **3a**, 2.810 ± 0.005 s; TFA 2.209 ± 0.002 s.

of the wide series of (hetero)arylboronates that we have tested to date,[18,21] with a half-life of < 0.003 s at 343 K. As shown below (Figure 10), even at 300 K the process is very rapid, with a half-life of just 0.12 seconds.

Using the interleaving technique, we analyzed the kinetics of the protodeboronation of **2b** at 300 K using stopped-flow ^{19}F NMR spectroscopy, Figure 10. With the reaction > 97% compete in 0.6 seconds, only a single data point can be obtained from each stopped-flow 'shot'. Consequently, θ was set to 90° to maximize the sensitivity, and a series of 10 shots interleaved. The phenomenological deadtime (0.22 s at a flow rate of 1 mL/s) resulted in the kinetics being analyzed for the last 20% of conversion. By increasing the flow rate to 2 mL/s, to achieve a phenomenological deadtime of 0.15 s, the activation parameters were able to be determined between 284 K and 323 K. We previously reported the rate of protodeboronation of **2b** at 343 K using the rapid quench flow technique.[21] At this temperature the rate of reaction is considerably faster than the phenomenological dead time of the stopped-flow NMR apparatus and the protodeboronation complete (> 99% **2b**→**3b**, in ≤ 0.02 s) before the first NMR pulse can be applied (0.15 s). Nonetheless, the data determined by stopped-flow NMR between 284 K and 323 K (red data points in Figure 11) correlate reasonably well with the rate determined by rapid quench flow at 343 K (blue datapoint).

Conclusions

We have demonstrated how using an insert that is compatible with a standard NMR spectrometer fitted with a He or N_2 cryoprobe, the stopped-flow NMR technique can be used to study the kinetics of rapid irreversible reactions such as the protodeboronation of 2,3,4,5,6-pentafluorophenyl boronate (**2b**, $t_{1/2}$ = 0.12 s at 300 K). Pre-magnetization coils (Figure 3) located close to the magnet core of the spectrometer induce about 90% polarization of the reagents before they are rapidly mixed (Figure 4) and enter the detection region. The design uses computer-controlled stepper-motor syringe drives to allow variable mixing ratios of reagents. The mixing time, pre-magnetization volumes, and phenomenological deadtime have also been assessed. The limiting reactant concentration for processes with large enthalpies of reaction, with sufficient thermostatting by the spectrometer to maintain approximately isothermal reaction kinetics has been evaluated by NMR cooling

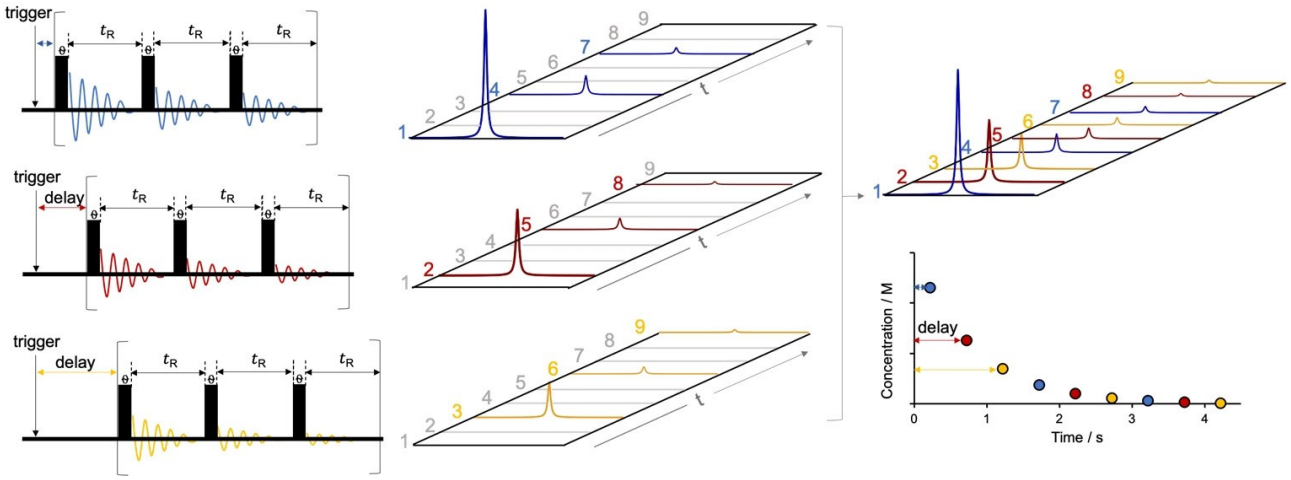

Figure 9. Schematic overview of the process of interleaving a series of spectra using an incremented trigger delay. The process effects manually enhanced temporal resolution when studying reactions that are too fast to acquire enough datapoints within a single 'shot' of the stopped-flow system. The three different colored subsets represent data obtained from identically initiated experiments; they are then combined to afford three-fold higher data density than the individual components.

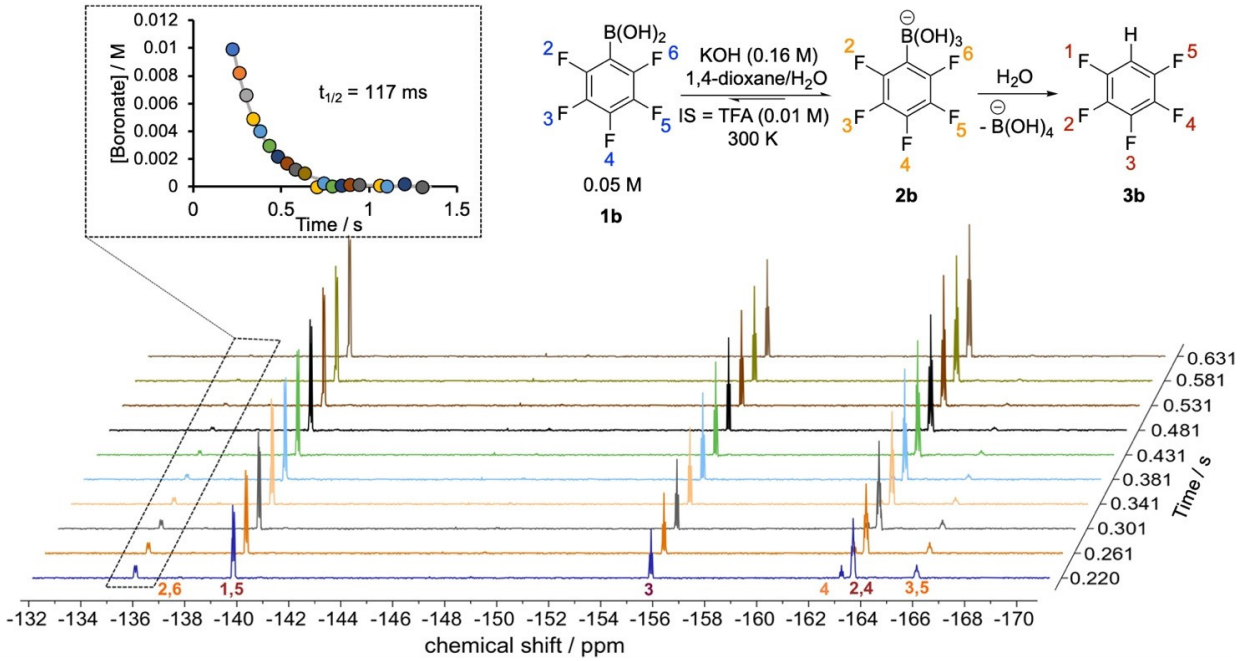

Figure 10. Interleaved ^{19}F stopped-flow spectra of the protodeboronation of 2,3,4,5,6-pentafluorophenyl boronic acid (**1b**) mediated by KOH in 1:1 dioxane/H_2O at 300 K. Inset: first-order decay of the boronate intermediate (**2b**), each differently-colored data point is generated from an interleaved set of two spectra, with an incremented trigger delay (only the first ten spectra are shown), grey line: non-linear regression to obtain the first-order rate constant, $k_{obs} = 5.9\ s^{-1}$; $t_{1/2} = 0.12$ s.

experiments, and mathematical modelling (Figure 5 and Figure 6). We have also conducted an evaluation of the key NMR parameters for quantitative analysis of the kinetics of relatively rapid irreversible reactions (equation 1, and Figure 7 and Figure 8). These parameters ensure sufficient nuclei relaxation between pulses, which is particularly important for reactions where the relaxation rate ($1/T_1$) is similar to, or smaller than, the reaction rate (k). Optimization of the pulse angle, θ, and interscan delay, t_R, allows the optimal balance between S/N and data density to be obtained. The data-density can also be manually enhanced by interleaving spectra (Figure 9 and Figure 10) from multiple experiments with different time offsets. We are currently developing an alternative design for stopped-flow NMR spectroscopy that affords significant reductions in the phenomenological dead-time, and are also measuring the rates of protodeboronation of polyfluorinated boronate esters,[47] relative to the corresponding boronic acids.[21,47] We will report in full on both of these investigations in due course.

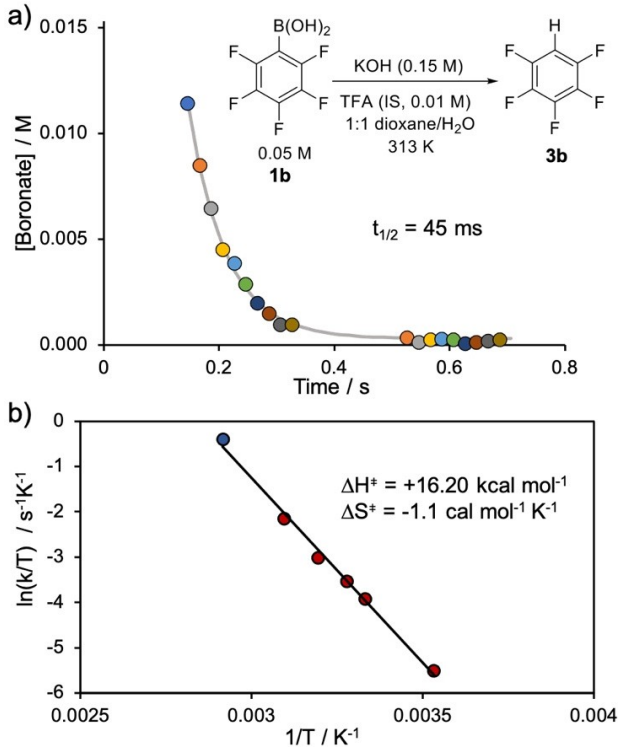

Figure 11. a) Base-catalyzed protodeboronation of pentafluorophenyl boronic acid (**1 b**) via the corresponding boronate **2 b** (See Figure 10) at 313 K ($t_{1/2}$ = 0.05 s). (b) Eyring analysis of rate data obtained by stopped-flow ^{19}F NMR analysis at 284 K, 300 K, 305 K, 313 K, and 323 K; the datapoint colored blue is a value previously determined by rapid quench flow, then ^{19}F NMR analysis (343 K; $t_{1/2}$ = 0.003 s).[21]

Experimental Section

NMR spectra were recorded on a 400 MHz Bruker Ascend spectrometer equipped with a 5 mm BBFO nitrogen cryoprobe. Stopped-flow experiments were performed with the custom built stopped-flow system, that we have previously outlined.[23] Temperature control in the pre-magnetization coils and mixer was achieved using a Huber Petite Fleur heater/chiller circulating a 50/50 ethylene glycol water mixture, with a Pt100 resistor terminated just below the mixer block. Temperature control of the reaction volume in the flow cell was achieved by use of the standard NMR spectrometer system in which dry air (or N_2) is passed up and around the sample. All NMR data were processed by Bruker TopSpin® 3.6.2 and MestReNova (version 14.0.0).

Pre-magnetization profiles measurement

Pre-magnetization profiles for three solution syringes were generated from ^{19}F stopped-flow experiments on samples of 0.1007 M 2-fluorophenyl boronic acid (T_1 = 1.649 ± 0.020 s) and 0.0999 M 4-fluorophenyl boronic acid (T_1 = 2.062 ± 0.021 s) in 1:1 dioxane/H_2O. Stock solutions were prepared separately to allow flexible control of variable input volumes. The pre-magnetization profile of each syringe was studied individually, during which time the studied syringe was filled with the stock solution and all other syringes with solvent. Input volumes from the syringe containing the stock solution were incremented from 50 µL to 900 µL in equal steps of 50 µL. For volumes < 600 µL, solvent was added from one of the other syringes to maintain a sufficient volume to flush the NMR tube. Each experiment was acquired with 3 loops of 90° pulses, and the interscan delay t_R was set to 15.76 s to ensure full relaxation recovery.

T_1-dependent polarization measurement

Pre-magnetization effects with respect to different T_1 constants were examined by interleaved ^{31}P stopped-flow experiments performed on a mixture of 0.5014 M PPh_3 (T_1 = 15.997 ± 0.001 s) and 0.5006 M O=PPh_3 (T_1 = 3.601 ± 0.001 s) in 9:1 THF/ H_2O. The pulse sequence shown in Figure 7a was used in 26 individual experiments with incremented trigger delays from 0.039 s to 44.04 s. Each experiment was acquired with 3 loops of 90° pulses, and the interscan delay t_R was set to 70.11 s to ensure full relaxation recovery.

Mixing time measurement

Mixing time measurements were performed using the Villermaux-Dushmann protocol.[48] Stock solutions of A) potassium iodide (0.032 M) and potassium iodate (0.006 M) in a sodium hydroxide/boric acid buffer (0.09 M) and B) sulfuric acid (0.06 M) were prepared. The stopped-flow instrument was prepared and primed with reagent line A containing the iodide/iodate stock solution, line B the sulfuric acid solution and line C containing distilled water. The waste line from the stopped-flow instrument was connected to a UV-Vis spectrometer flow cell with a 5 mm path length. For each mixing time measurement, syringes A and B were driven at a constant flow rate for the full volume (2.5 mL per syringe). For measurements using three syringes, line C was filled with the sulfuric acid solution and the three syringes were driven in a 2:1:1 ratio (2.5:1.25:1.25 mL). The absorbance at 353 nm was monitored until a stable signal was observed, with the final absorbance measured after the flow was stopped. The measurements were repeated three times at each flow rate and averaged. Mixing times and power dissipation were estimated from the measured absorbance values using the master curve reported by Falk *et. al.*:[48]

$$t_m = 0.33 \times (absorbance) \times [H^+]^{-4.55}[KI]^{-1.5}[KIO_3]^{5.8}[NaOH]^{-2}[H_3BO_3]^{-2}$$

$$t_m = 0.15\ \varepsilon^{-0.45}$$

$$t_{m\ (theoretical)} = \frac{d}{8\,\bar{u}}\,\mathrm{arcsinh}(0.76\ Pe)$$

Where t_m is the mixing time (s), ε is the dissipated power (W.kg^{-1}), d is the characteristic diameter of the mixer (m), ū is the mean velocity of the fluid (m.s^{-1}) and *Pe* is the Peclet number (proportional to Reynolds number).

Protodeboronation of 2,3,4,6-tetrafluorophenyl boronic acid 1 a

A stock solution of 0.083 M 2,3,4,6-tetrafluorophenyl boronic acid (T_1 = 1.347 ± 0.009 s for signal δ = −109 ppm) and 0.0197 M trifluoroacetic acid (IS) (T_1 = 2.123 ± 0.004 s before reaction and T_1 = 2.209 ± 0.002 s after reaction, δ = −76 ppm, CF_3CO_2K) was freshly prepared in 1:1 dioxane/H_2O. A solution of 0.3022 M (3 equivalent) of KOH in 1:1 dioxane/H_2O was prepared separately. T_1 constants of ^{19}F nuclei in the starting materials and product were measured individually in the flow-cell of the stopped flow system using standard 'inversion recovery' experiments (see SI for full details). The reaction was initiated by simultaneously inputting 300 µL of

boronic acid and 300 μL of base solution from syringe A and syringe B, at a flow rate of 1 mL/s. ^{19}F NMR spectra were then acquired with a minimum trigger delay of 0.039 s. The interscan delay was 1.36 s (relaxation delay of 0.5 s and acquisition time of 0.8 s respectively) for 10° pulses, and 1.86 s (relaxation delay of 1 s and acquisition time of 0.8 s respectively) for 45° and 90° pulses.

Protodeboronation of 2,3,4,5,6-pentafluorophenyl boronic acid 1 b

A stock solution of 0.0993 M 2,3,4,5,6-pentafluorophenyl boronic acid ($T_1 = 0.636 \pm 0.005$ s for signal $\delta = -134$ ppm) and 0.0261 M trifluoroacetic acid (IS) was freshly prepared in 1:1 dioxane/H_2O. A solution of KOH 0.3212 M (3 equivalent) in 1:1 dioxane/H_2O was prepared separately. The thermostats on the spectrometer and auxiliary system were both set to 300 K. The reaction was initiated by computer-controlled simultaneous delivery of 300 μL of the boronic acid solution, and 300 μL of base solution, at a flow rate of 1 mL/s. Interleaved ^{19}F NMR spectra were acquired with incremented trigger delays of 0.039, 0.08, 0.12, 0.16, 0.20, 0.25. 0.30, 0.35, 0.4, and 0.45 s. The interscan delay was 0.36 s, and the pulse angle was 60°.

A solution of 0.1031 M 2,3,4,5,6-pentafluorophenyl boronic acid and 0.0246 M trifluoroacetic acid (IS) was freshly prepared in 1:1 dioxane/H_2O. A solution of KOH 0.2994 M (3 equivalent) in 1:1 dioxane/H_2O was prepared separately. The thermostats on the spectrometer and auxiliary system were both set to 313 K. The reaction was initiated by computer-controlled simultaneous delivery of 300 μL of the boronic acid solution, and 300 μL of base solution, at a flow rate of 2 mL/s. Interleaved stopped-flow spectra were acquired with incremented trigger delays of 0.039, 0.06, 0.08, 0.10, 0.12, 0.14. 0.16, 0.18, 0.20, and 0.22 s. The interscan delay was 0.36 s, and the pulse angle was 90°.

Acknowledgements

Professor Erik von Harbou (Kaiserslautern) facilitated the visit of R.B. to Edinburgh and provided assistance in the calculations of heat-transfer coefficients and reaction thermodynamics. Dr. Andrew Leach (Manchester) conducted the DFT calculations on the reaction enthalpies for protodeboronation. Professor John Blacker (Leeds) made very useful suggestions regarding estimates of mixing efficiency and the use of the Villermaux-Dushmann protocol. Dr. Ruth Dooley, Dr. Ariana Jones and Professor Dušan Uhrín (Edinburgh) made numerous valuable contributions and suggestions in the early stages of this project; Hannah Hayes (Edinburgh) provided detailed advice for the studies of the kinetics of the protodeboronation reactions.

Conflict of Interest

The authors declare no conflict of interest.

Keywords: Kinetics · NMR spectroscopy · Protodeboronation · Rapid reactions · Stopped-flow

[1] B. A. Abel, C. A. L. Lidston, G. W. Coates, *J. Am. Chem. Soc.* **2019**, *141*, 12760–12769.
[2] D. G. Blackmond, *J. Am. Chem. Soc.* **2015**, *137*, 10852–10866.
[3] F. Susanne, D. S. Smith, A. Codina, *Org. Process Res. Dev.* **2012**, *16*, 61–64.
[4] H. S. Gutowsky, A. Saika, *J. Chem. Phys.* **1953**, *21*, 1688–1694.
[5] H. M. McConnell, *J. Chem. Phys.* **1958**, *28*, 430–431.
[6] J. Kaplan, P. P. Yang, G. Fraenkel, *J. Chem. Phys.* **1974**, *60*, 4840–4845.
[7] S. Forsén, R. A. Huffman, *J. Chem. Phys.* **1963**, *39*, 2892–2901.
[8] J. Jeener, B. H. Meier, P. Bachmann, R. R. Ernst, *J. Chem. Phys.* **1979**, *71*, 4546–4553.
[9] Z. Luz, S. Meiboom, *J. Chem. Phys.* **1963**, *39*, 366–370.
[10] A. Allerhand, H. S. Gutowsky, *J. Chem. Phys.* **1964**, *41*, 2115–2126.
[11] A. Allerhand, H. S. Gutowsky, *J. Chem. Phys.* **1965**, *42*, 1587–1599.
[12] H. Y. Carr, E. M. Purcell, *Phys. Rev.* **1954**, *94*, 630–638.
[13] S. Meiboom, D. Gill, *Rev. Sci. Instrum.* **1958**, *29*, 688–691.
[14] A. B. Jones, G. C. Lloyd-Jones, D. Uhrín, *Anal. Chem.* **2017**, *89*, 10013–10021.
[15] D. D. Boehr, H. J. Dyson, P. E. Wright, *Chem. Rev.* **2006**, *106*, 3055–3079.
[16] A. Mittermaier, L. E. Kay, *Sci. J.* **2006**, *312*, 224–228.
[17] Y. Ji, D. A. DiRocco, C. M. Hong, M. K. Wismer, M. Reibarkh, *Org. Lett.* **2018**, *20*, 2156–2159.
[18] P. A. Cox, A. G. Leach, A. D. Campbell, G. C. Lloyd-Jones, *J. Am. Chem. Soc.* **2016**, *138*, 9145–9157.
[19] A. J. J. Lennox, G. C. Lloyd-Jones, *J. Am. Chem. Soc.* **2012**, *134*, 7431–7441.
[20] J. A. Gonzalez, O. M. Ogba, G. F. Morehouse, N. Rosson, K. N. Houk, A. G. Leach, P. H.-Y. Cheong, M. D. Burke, G. C. Lloyd-Jones, *Nat. Chem.* **2016**, *8*, 1067–1075.
[21] P. A. Cox, M. Reid, A. G. Leach, A. D. Campbell, E. J. King, G. C. Lloyd-Jones, *J. Am. Chem. Soc.* **2017**, *139*, 13156–13165.
[22] E. Kühnel, D. D. P. Laffan, G. C. Lloyd-Jones, T. Martínez Del Campo, I. R. Shepperson, J. L. Slaughter, *Angew. Chem. Int. Ed.* **2007**, *46*, 7075–7078; *Angew. Chem.* **2007**, *119*, 7205–7208.
[23] C. P. Johnston, T. H. West, R. E. Dooley, M. Reid, A. B. Jones, E. J. King, A. G. Leach, G. C. Lloyd-Jones, *J. Am. Chem. Soc.* **2018**, *140*, 11112–11124.
[24] A. García-Domínguez, T. H. West, J. J. Primozic, K. M. Grant, C. P. Johnston, G. G. Cumming, A. G. Leach, G. C. Lloyd-Jones, *J. Am. Chem. Soc.* **2020**, *142*, 14649–14663.
[25] L. T. Ball, T. J. A. Corrie, A. J. Cresswell, G. C. Lloyd-Jones, *ACS Catal.* **2020**, *10*, 10420–10426.
[26] H. J. A. Dale, C. Nottingham, C. Poree, G. C. Lloyd-Jones, *J. Am. Chem. Soc.* **2021**, *143*, 2097–2107.
[27] F. Song, R. D. Cannon, M. Bochmann, *J. Am. Chem. Soc.* **2003**, *125*, 7641–7653.
[28] T. E. Barman, S. R. W. Bellamy, H. Gutfreund, S. E. Halford, C. Lionne, *Cell. Mol. Life Sci. C.* **2006**, *63*, 2571–2583.
[29] J. F. Eccleston, S. R. Martin, M. J. Schilstra, in *Biophys. Tools Biol. Vol. One Vitr. Tech.*, Academic Press, **2008**, pp. 445–477.
[30] J. F. McGarrity, C. A. Ogle, Z. Brich, H. R. Loosli, *J. Am. Chem. Soc.* **1985**, *107*, 1810–1815.
[31] K. H. Mok, T. Nagashima, I. J. Day, J. A. Jones, C. J. V. Jones, C. M. Dobson, P. J. Hore, *J. Am. Chem. Soc.* **2003**, *125*, 12484–12492.
[32] S. E. Denmark, B. M. Eklov, P. J. Yao, M. D. Eastgate, *J. Am. Chem. Soc.* **2009**, *131*, 11770–11787.
[33] R. Franco, A. Favier, P. Schanda, B. Brutscher, *J. Magn. Reson.* **2017**, *281*, 125–129.
[34] S. E. Denmark, B. J. Williams, B. M. Eklov, S. M. Pham, G. L. Beutner, *J. Org. Chem.* **2010**, *75*, 5558–5572.
[35] S. Bowen, C. Hilty, *Phys. Chem. Chem. Phys.* **2010**, *12*, 5766–5770.
[36] J. Grimaldi, J. Baldo, C. McMurray, B. D. Sykes, *J. Am. Chem. Soc.* **1972**, *94*, 7641–7645.
[37] J. J. Grimaldi, B. D. Sykes, *Rev. Sci. Instrum.* **1975**, *46*, 1201–1205.
[38] R. O. Kühne, T. Schaffhauser, A. Wokaun, R. R. Ernst, *J. Magn. Reson.* **1979**, *35*, 39–67.
[39] S. Funahashi, K. Ishihara, S. I. Aizawa, T. Sugata, M. Ishii, Y. Inada, M. Tanaka, *Rev. Sci. Instrum.* **1993**, *64*, 130–134.
[40] P. V. Yushmanov, I. Furó, *J. Magn. Reson.* **2005**, *175*, 264–270.
[41] M. D. Christianson, E. H. P. Tan, C. R. Landis, *J. Am. Chem. Soc.* **2010**, *132*, 11461–11463.
[42] A. L. Dunn, C. R. Landis, *Magn. Reson. Chem.* **2017**, *55*, 329–336.
[43] E. von Harbou, R. Behrens, J. Berje, A. Brächer, H. Hasse, *Chem. Ing. Tech.* **2017**, *89*, 369–378.

[44] A. Scheithauer, A. Brächer, T. Grützner, D. Zollinger, W. R. Thiel, E. von Harbou, H. Hasse, *Ind. Eng. Chem. Res.* **2014**, *53*, 17589–17596.
[45] M. D. Christianson, C. R. Landis, *Concepts Magn. Reson. Part A* **2007**, *30 A*, 165–183.
[46] A. García-Domínguez, P. H. Helou de Oliveira, G. T. Thomas, A. R. Sugranyes, G. C. Lloyd-Jones, *ACS Catal.* **2021**, *11*, 3017–3025.
[47] Y. P. Budiman, S. A. Westcott, U. Radius, T. B. Marder, *Adv. Synth. Catal.* **2021**, *363*, DOI 10.1002/adsc.202001291.
[48] J.-M. Commenge, L. Falk, *Chem. Eng. Process. Process Intensif.* **2011**, *50*, 979–990.
[49] L. Falk, J.-M. Commenge, in *Micro Process Eng.*, Wiley-VCH Verlag GmbH & Co. KGaA, Weinheim, Germany, **2013**, pp. 145–173.
[50] L. Falk, J.-M. Commenge, *Chem. Eng. Sci.* **2010**, *65*, 405–411.
[51] C.-Y. Lee, W.-T. Wang, C.-C. Liu, L.-M. Fu, *Chem. Eng. J.* **2016**, *288*, 146–160.
[52] On exiting the mixer, the nascent reaction mixture is transported to the flow-cell via a narrow-bore glass capillary that passes through the liquid heat-transfer medium thus dissipating any significant enthalpy of mixing.
[53] C. Ammann, P. Meier, A. Merbach, *J. Magn. Reson.* **1982**, *46*, 319–321.
[54] D. A. Foley, E. Bez, A. Codina, K. L. Colson, M. Fey, R. Krull, D. Piroli, M. T. Zell, B. L. Marquez, *Anal. Chem.* **2014**, *86*, 12008–12013.
[55] R. R. Ernst, W. A. Anderson, *Rev. Sci. Instrum.* **1966**, *37*, 93–102.
[56] Estimated enthalpies have previously been reported, using DFT methods.[21] The enthalpy change for the initial conversion to the boronate (**1a**→**2a**) is calculated to be larger, about -1.6×10^2 kJmol^{-1}. However this equilibrium process proceeds extremely rapidly[14] and is complete within the timescale of mixing, under control of the auxiliary thermostat.[52]

Manuscript received: March 8, 2021
Revised manuscript received: March 25, 2021
Accepted manuscript online: March 26, 2021